This is a peer reviewed version of an article published in *Chemosphere*, 199, 68-75 (2018). The published version is available online at: https://doi.org/10.1016/j.chemosphere.2018.01.174

Heterogeneous electro-Fenton as plausible technology for the degradation of imidazolinium-based ionic liquids

V. Poza-Nogueiras[a], M. Arellano[a], E. Rosales[a], M. Pazos[a], E. González-Romero[b]*, M. A. Sanromán[a]*

[a]Department of Chemical Engineering, University of Vigo, Campus Lagoas-Marcosende, 36310 Vigo, Spain

[b]Department of Analytical and Food Chemistry, University of Vigo, Campus Lagoas-Marcosende, 36310 Vigo, Spain

**Corresponding authors.*

Tel: +34986812383; fax: +34986812380; E-mail: sanroman@uvigo.es

(M. Angeles Sanromán)

Tel: +34986812240; fax: +34986812380; E-mail: eromero@uvigo.es

(Elisa González-Romero)

ABSTRACT

Conventional water treatments are generally inadequate for degradation of emerging pollutants such as ionic liquids (ILs). The use of heterogeneous electro-Fenton (HEF) has attracted great interest, due to its ability to efficiently oxidize a wide range of organic pollutants operating in cycles or in continuous mode. In this study, the removal of a complex IL from the imidazolinium family (1,3-Bis(2,4,6-trimethylphenyl)imidazolinium chloride, by means of HEF using iron alginate spheres as catalyst has been investigated, resulting in significant TOC decay after 6 h. The optimization of the key process parameters (current, IL concentration and catalyst dosage) has been performed using a Box-Behnken experimental design and achieving 76.98% of TOC abatement in 2 h of treatment. Current proved to be a crucial parameter and high catalyst dosage is required to achieve the maximum removal. In addition, an insight about the availability of iron into the reactor and the evolution of several intermediates has been carried out by employing Differential Pulse Voltammetry on Screen-Printed Carbon Electrodes. The evolution of the different voltammetric peaks confirmed the influence of iron release, and the generation of several iron complexes has permitted the

comprehension of the degradation pathway, which has been validated by chromatographic techniques.

Keywords: 1,3-Bis(2,4,6-trimethylphenyl)imidazolinium chloride; heterogeneous catalysis; heterogeneous electro-Fenton; iron alginate spheres; Differential Pulse Voltammetry; Screen-Printed Carbon Electrode.

1. INTRODUCTION

Ionic liquids (ILs) are organic salts with low vapor pressure, melting point and flammability that have attracted attention, in recent years, as 'green' replacements for industrial volatile compounds in applications such as catalysts, biocatalysts, biotechnology, synthetic chemistry and electrochemistry (Dai et al., 2017). Although they are considered as green solvents due to their low volatility, they are highly water-soluble and chemically and thermally stable. This fact, together with their complex chemical structure, that involves a cationic or anionic polar head group with accompanying alkyl side chains, creates the potential for entry and persistence in the environment (Deive et al., 2011). Kalcikova et al. (2012) compared the ecotoxicity of 1-butyl-3-methylpyridinium dicyanamide to other commonly used solvents, and found it to be toxic to all organisms tested and even more toxic than common solvents. Current data highlights this problem and shows that ILs are toxic in nature and that their toxicities vary considerably across organisms and trophic levels (Egorova and Ananikov, 2014). Therefore, they are considered as "Contaminants on the Horizon" (Richardson and Kimura, 2017).

In this context, processes that could be effective are required to deal with these non-readily biodegradable and toxic pollutants (Pęziak-Kowalska et al., 2017). Several processes as photodegradation, ultrasonic, electrochemical or Fenton (Muñoz et al., 2015; Morandeira et

al., 2017; Mena et al., 2018) have been tested in order to degrade different families of ILs contained in water. Table 1 summarizes some recent research on this topic. Among all the degradation techniques, electro-Fenton (EF) process is one of the most known and popular (Sirés et al., 2014). Recently, this process has been evaluated for the removal of ILs; however, to our knowledge, there are only few studies reported in the literature about this issue (Bocos et al., 2016; Garcia-Segura et al., 2016). In EF, the degradation reaction of the anodic oxidation is enhanced by the generation of the hydroxyl radical from the reaction of electrogenerated H_2O_2 with Fe^{2+}, which can be considered as catalyst. Due to the application of electric field, the Fe^{3+} generated in the process is regenerated to Fe^{2+}.

Table 1. Recent research on ILs degradation

IL	Degradation process[1]	IL elimination	Mineralization[2]	Ref.
a) 1-Ethyl-3-methylimidazolium chloride b) 1-Butyl-4-methypyridinium chloride c) Tetrabutylammonium chloride d) Tetrabutylphosphonium chloride (1 g L^{-1})	F	100% (<10 min)	TOC / COD decay (4 h): a) 65% / 78% b) 45% / 64% c) 43% / 63% d) 28% / 50%	Muñoz et al. (2015)
a) 1-Hexyl-3-methylimidazolium dicyanamide b) 1-Butyl-3-methylimidazolium dicyanamide c) 1-Ethyl-3-methylimidazolium dicyanamide d) 1-Ethyl-3-methylimidazolium acetate e) 1-Ethyl-3-methylimidazolium methylsulfate (0.5 g L^{-1})	HEF	100% (2 h)	TOC decay (8 h): a) 80% b) 85% c) 100% (6 h) d) 100% e) 100%	Bocos et al. (2016)
a) 1-Butyl-4-methylpyridinium chloride (0.83 mM) b) 1-Ethyl-3-methylimidazolium chloride (1.39 mM)	E-H_2O_2 EF PEF	-	DOC decay (6 h): a) 97% (E- H_2O_2), 91% (EF), 97% (PEF) b) 94% (E- H_2O_2), 93% (EF), 94% (PEF)	Garcia-Segura et al. (2016)
a) 1-Ethyl-3-methylimidazolium chloride b) 1-Butyl-3-methylimidazolium chloride c) 1-Octyl-3-methylimidazolium chloride d) 1-Hexadecyl-3-methylimidazolium chloride (1 g L^{-1})	HF	100% (1 h)	TOC decay (4 h): a) 44% b) 38% c) 36% d) 33%	Muñoz et al. (2016)
1-Butyl-3-methylimidazolium triflate (0.5 g L^{-1})	EF	100% (45 min)	100% TOC decay (45 min)	Bocos et al. (2017)

(2-Hydroxyethyl)trimethylammonium chloride (Choline chloride, 1mM)	B	100% (<24 h)	-	Morandeira et al. (2017)
Didecyldimethylammonium (4-chloro-2-methylphenoxy)acetate (0.05 g L^{-1})	EF E	100% (15 min)	TOC / COD decay (6 h): 80% / 95% (EF) 30% / 50% (E)	Pęziak-Kowalska et al. (2017)
a) 1-Hexyl-3-methylimidazolium chloride b) 1-Butyl-4-methylpyridinium chloride (1 g L^{-1})	F	a) 100% (30 min) b) 100% (2 h)	TOC decay (4 h): a) 54% b) 44%	Gomez-Herrero et al. (2018)
1-Butylpyridinium chloride (0.5 g L^{-1})	HEF	100% (2 h)	TOC / COD decay (8 h): 94% / 95%	Meijide et al. (2018)
1-Butyl-3-methylimidazolium bis(trifluoromethanesulfonyl)imide (0.419 g L^{-1})	E E-H_2SO_4 SE PE	-	TOC decay (8 h): 68% (E) 81% (E-H_2SO_4) 78% (SE) 76% (PE)	Mena et al. (2018)

[1]**B**: biotechnology; **E**: electrolysis; **EF**: electro-Fenton; **F**: Fenton; **HEF**: heterogeneous electro-Fenton; **HF**: heterogeneous Fenton; **PE**: photoelectrolysis; **PEF**: photoelectro-Fenton; **SE**: sonoelectrolysis.

[2]**COD**: chemical oxygen demand; **DOC**: dissolved organic carbon; **TOC**: total organic carbon.

Heterogeneous iron catalyst has a number of benefits, such as it can be easily and effectively recovered from a reaction mixture in a straightforward manner and reused in other cycles or permits the operation in continuous mode, which is an important consideration for industrial manufacturing processes. Nowadays, to perform heterogeneous iron catalyst processes several strategies are leading such as use of iron-based solid particles (pyrite, magnetite, wustite, chalcopyrite) (Barhoumi et al., 2015; Barhoumi et al., 2017; Ouiriemmi et al., 2017) or by hosting on different supports (alginate, sepiolite, kaolinite) (Iglesias et al., 2013; Bocos et al., 2014). In several of these heterogeneous processes, the catalyst is used as iron reservoir for constant dosing of homogenous iron catalyst avoiding the negative effect of the use of high iron concentration. To understand the mechanisms that take place in these heterogeneous processes and to improve the efficiency of the EF treatment it is necessary to apply analytical tools, such as the voltammetric technique, to partially elucidate the evolution of iron into the solution and the degradation mechanism of the pollutants that permit a rapid decision-making. Recently, a study published by Bocos et al. (2017) has demonstrated the potentialities of this

methodology identifying the formation of iron complex intermediates during the treatment of 1-butyl-3-methylimidazolium triflate by EF process. However, this tool has never been used for monitoring the degradation of ILs by heterogeneous EF (HEF).

For those reasons, this study is focused on the application of HEF using iron alginate gel spheres (FeAS) as catalyst for the degradation of a complex IL from imidazolinium family (1,3-Bis(2,4,6-trimethylphenyl)imidazolinium chloride, [IMes.HCl]). Furthermore, this work is focused on the development of two innovative milestones: i) verification and optimization of the HEF process to treat [IMes.HCl], and ii) application of Screen-Printed Carbon Electrodes (SPCE) as transducer from Differential Pulse Voltammetry (DPV) analysis that permits the *in situ* monitoring of the process.

2. MATERIALS AND METHODS

2.1. Chemicals

1,3-Bis(2,4,6-trimethylphenyl)imidazolinium chloride [IMes.HCl], $C_{21}H_{27}ClN_2$ (Fig. SM-1), Na_2SO_4, $Fe_2(SO_4)_3xH_2O$ and H_2SO_4 were purchased from Sigma-Aldrich. Sodium alginate was provided by Analema. HPLC and IC mobile phases were prepared with H_2SO_4 HPLC grade (Sigma-Aldrich) and Na_2CO_3 and $NaHCO_3$ (both from Fluka), respectively. All solutions were prepared with Millipore filtered water.

2.2. Iron alginate gel spheres (FeAS)

A 2.0% (w/v) sodium alginate solution was prepared and dropped through a syringe from an approximate distance of 20 cm into an agitated hardening solution composed of 0.05 M $Fe_2(SO_4)_3xH_2O$ in order to fix the iron into spherical alginate beads (Iglesias et al., 2014).

2.3. HEF treatment

HEF experiments were carried out in an open and undivided cylindrical glass reactor with 0.15 L of the IL solution and Na_2SO_4 (0.01 M) at pH 3 with continuous bubbling of air (0.5 L

min^{-1}) on the cathode surface for *in situ* generation of H_2O_2. FeAS were placed inside a basket tailored with a plastic net to prevent their breaking down.

A constant current was applied via two electrodes connected to a direct power supply (HP-model 3662). The cathode, a carbon felt electrode (18.5 cm x 5.0 cm, Carbon-Lorrain), was placed on the inner wall of the cell covering the totality of the internal perimeter. The anode, a boron-doped diamond (BDD) electrode (5.0 cm x 2.5 cm, DiaChem) with a 4-5 μm diamond thickness and a doping level around 2500 ppm, was located in the center of the reactor. The process was monitored with a multimeter (Fluke 175).

2.4. Analytical methods

2.4.1. [IMes.HCl] concentration and mineralization

[IMes.HCl] was determined by the absorbance at the maximum wavelength of 248 nm using a UV-visible spectrophotometer (Jasco V-630). The IL mineralization was monitored through the TOC content. It was measured via catalytic high-temperature combustion by multi N/C 3100 equipment (Analytic Jena) coupled with a non-dispersive infrared detector (C.A.C.T.I., University of Vigo).

2.4.2. IC and HPLC analysis

An ion chromatographic system with conductimetric detection was used to analyze mainly the inorganic anions generated during the HEF treatment. The chromatographic system, Metrohm 792 Basic IC chromatograph equipped with a 20 μL loop Rheodyne injection valve, was operated with chemical suppression mode. The column was a 250 mm x 4 mm Metrosep A supp 4. The eluent was a 1.8 mM Na_2CO_3 and 1.7 mM $NaHCO_3$ solution (standard flow of 1 mL min^{-1}), which was degassed during 30 min before use.

Identification of carboxylic acids was performed with an ion-exclusion HPLC using Agilent 1100 HPLC equipped with a Rezex™ ROA-Organic Acid H+ (8%) column (300 mm x 7.8 mm; Phenomenex). The working temperature of the column was 60ºC and the mobile phase,

H_2SO_4 (5 mM), was flow at 0.5 mL min^{-1}. Identification of the organic acids was made by comparing the retention time and UV spectra of the samples with those of pure standards.

2.4.3. Voltammetric analysis

Cyclic Voltammetry (CV) and DPV were applied for electrode surface activation and IL degradation measurements, respectively, using a potentiostat/galvanostat AUTOLAB PGSTAT 30 controlled by the General Purpose Electrochemical Experiments Software (GPES 4.9.05) and a DropSens DSC connector. The electrochemical cell configuration consists in an SPCE (DRP C110, DropSens), composed by a carbon working electrode with a 4 mm diameter, an Ag-pseudo-reference electrode and a carbon counter electrode. For each measurement, 50 µL of solution were dispensed on the SPCE.

DPV was used for monitoring the evolution of electroactive compounds from the HEF process. The DPV conditions were as follows: step potential of 5 mV; pulse amplitude of 50 mV, modulation time of 0.05 s, interval time of 0.5 s and scan rate of 9.9 mV s^{-1}. Typically, the working window potential was scanned from +0.8 V to -0.5 V to monitor the Fe(III) electrochemical reduction process.

An "activation/cleaning" step of the working SPCE was performed previous to the measurement and between successive runs in order to activate the electrode surface and remove any impurity from it. For doing so, 5 cycles by CV in the potential range from −1.2 to +1.2 V at 100 mV s^{-1} in 0.05 M H_2SO_4 solution were applied.

2.5. Experimental design and statistical analysis

Box-Behnken experimental design for response surface methodology (RSM) has been used for optimizing several engineering processes. The design was composed by three factors studied in three levels and 17 runs were carried out in duplicate to optimize the level of the chosen variables: current (X_1), FeAS dosage (X_2) and IL concentration (X_3) (Table 2).

The statistical analysis of this model was performed in order to assess the analysis of variance (ANOVA) using Design Expert® 8.0.0 software (Stat-Ease Inc. Minneapolis, USA). In the RSM, a quadratic equation (1) is usually applied to correlate the relationship between the predicted response and the independent variables in coded values:

$$Y_i = \beta_0 + \sum \beta_i X_i + \sum \beta_{ii} X_i^2 + \sum \beta_{ij} X_i X_j \qquad (1)$$

where Y_i is the response, β_0 is a constant, β_i is the slope or linear effect of the input factor, β_{ii} is the quadratic effect, β_{ij} is the two-way linear by linear interaction effect and X_i and X_j are the independent parameters (Simsek et al., 2013).

3. RESULTS AND DISCUSSION

3.1. HEF

Initially, the HEF process was evaluated operating with 1 g of FeAS at 150 mA for the degradation of [IMes.HCl] at initial concentration of 0.5 mM. The evolution of IL degradation followed a pseudo first-order kinetic model ($k = 0.0265$ min^{-1}, $R^2 = 0.994$) and the TOC reduction achieved was 85.67% after 6 h. To improve the HEF, it is necessary to evaluate the effect of operational parameters and therefore, RSM was adopted to design the experiments.

An experimental design based on a Box-Behnken method in RSM was proposed to evaluate the role played by key parameters of HEF such as current, catalyst dosage and IL concentration. Table 2 presents the design matrix of the variables in natural units and the analytical response corresponds to the TOC reduction level after 2 h of reaction time.

3.1.1 Statistical ANOVA analysis

Table 3 shows the results of the ANOVA analysis, which is essential to test significance and adequacy of the model. As shown in Table 3, the F-value (23.4), combined with the low p-value (p-values<0.0001) implies that the model is statistically significant; this indicates that the model fitted well to predict the outcome variable and that there is a significant relationship between the set of predictors and the dependent variable. The coefficient of determination

(R^2) and adjusted R^2 value were 0.9141 and 0.8750, respectively, which are in reasonable agreement. In addition, the signal to noise ratio was measured by the Adequate Precision, obtaining a ratio of 18.855 that indicates an adequate signal. Furthermore, Coefficient of Variation was lower than 15%, limit proposed by Rossi (2010) to indicate a greater reliability of the experiments performed. Therefore, the obtained data can be fitted to a model following equation (2) using the coded values.

$$\text{TOC removal (\%)} = 65.33 + 8.33 \cdot X_1 + 5.0 \cdot X_2 - 5.40 \cdot X_3 + 9.04 \cdot X_1X_3 - 9.08 \cdot X_1^2 \quad (2)$$

In the perturbation plot (Fig. SM-2a), it can be observed in the curvature (factor X_1) and steep slope (factors X_2 and X_3) that the response is sensitive to that factors. However, interaction between the factors cannot be analysed using this plot and therefore Pareto chart was considered (Fig. SM-2b). The results show that the three variables (X_1, X_2, X_3), the square of current (X_1^2) and the interaction between this variable with IL concentration (X_{13}) have a strong effect on the TOC reduction, which is in accordance with the data displayed in Table 3.

Table 2. Design matrix for HEF process, including the coded levels, independent variables and response.

Run	Current (mA)	FeAS dosage (g)	Ionic liquid concentration (mg C L^{-1})	TOC reduction (%)
1	300.00 (+1)	3.00 (0)	50.00 (-1)	61.74
2	50.00 (-1)	3.00 (0)	200.00 (+1)	36.34
3	175.00 (0)	5.00 (+1)	200.00 (+1)	60.98
4	175.00 (0)	1.00 (-1)	200.00 (+1)	58.17
5	175.00 (0)	1.00 (-1)	50.00 (-1)	71.30
6	300.00 (+1)	3.00 (0)	200.00 (+1)	72.77
7	175.00 (0)	3.00 (0)	125.00 (0)	63.99
8	175.00 (0)	5.00 (+1)	50.00 (-1)	76.93
9	175.00 (0)	3.00 (0)	125.00 (0)	64.22
10	50.00 (-1)	1.00 (-1)	125.00 (0)	37.40
11	175.00 (0)	3.00 (0)	125.00 (0)	63.94
12	50.00 (-1)	3.00 (0)	50.00 (-1)	61.49

13	175.00 (0)	3.00 (0)	125.00 (0)	64.09
14	300.00 (+1)	5.00 (+1)	125.00 (0)	68.15
15	175.00 (0)	3.00 (0)	125.00 (0)	64.35
16	300.00 (+1)	1.00 (-1)	125.00 (0)	55.69
17	50.00 (-1)	5.00 (+1)	125.00 (0)	56.46

Table 3. ANOVA analysis for response surface.

Source	**Sum of squares**	**Degrees of freedom**	**Mean square**	**F values**	***p*-values**
Model	1664.37	5	332.87	23.40	<0.0001
X_1-Current	555.44	1	555.44	39.05	<0.0001
X_2-FeAS dosage	199.60	1	199.60	14.03	0.0032
X_3-[IL]	233.28	1	233.28	16.40	0.0019
X_1 X_3	327.25	1	327.25	23.00	0.0006
X_1^2	348.80	1	348.80	24.52	0.0004
Standard Deviation: 3.77		Mean: 61.06		Coefficient of Variation (%): 6.18	
Adequate Precision: 18.855		R^2: 0.9141		Adjusted R^2: 0.8750	

3.1.2 RSM

The response surface plot for TOC reduction is represented in Fig. 1, as a function of current and IL concentration while the catalyst dosage was kept constant at the central level. It is detected that the TOC reduction increases when the IL concentration decreases, and at the highest concentration the removal levels are increased proportional to the current. Thus, the current is a crucial parameter since it governs the electrochemical processes and in EF regulates the amount of physisorbed oxidative radicals on cathode surface that oxidizes the present pollutants up to degradation (Guelfi et al., 2017).

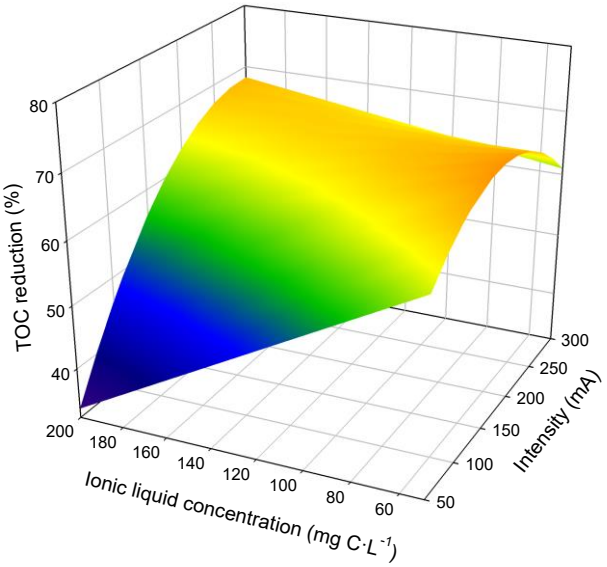

Fig. 1. Response surface plot showing the effect of current and IL concentration on TOC reduction at the end of 2 h keeping the FeAS at the central value.

Based on our results, the TOC reduction levels at high current were higher than those obtained at low current. This can be explained considering the larger amount of •OH physisorbed on BBD surface and in the bulk solution produced when the applied current was increased. However, at low IL concentration the reduction of the level achieved is observed. This fact can be explained considering that when a low concentration of IL was used the high current applied generated an excess of these radicals that could be also consumed in scavenger no-oxidation reactions (equations (3) and (4)) that reduce the current efficiency (Mousset et al., 2014; Lin et al., 2017).

$$2BDD(\bullet OH) \rightarrow 2BDD + O_2 + 2H^+ + 2e^- \quad (3)$$

$$2BDD(\bullet OH) \rightarrow 2BDD + H_2O_2 \quad (4)$$

3.1.3 Optimization of the significant factors

The optimization of the operational conditions was carried out based on the desirability function, and the optimal conditions were obtained based on the model: current 170.25 mA,

FeAS dosage 5 g, and LI concentration 50 mg C L^{-1}. As result of this model, a theoretical TOC reduction of 75.74% was determined.

To confirm the adequacy of the model for predicting the maximum TOC reduction, a confirmation assay was performed. The obtained results reached 76.98% of TOC reduction after 2 h of treatment. This value means a good agreement between the predicted and the experimental values with a deviation lower than 2%. This result confirms the validation of the model for the IL degradation.

Based on the obtained results, it is clear that it is necessary to know the pathway of the reactions that take place in this process in order to provide a rapid decision-making to improve the efficiency of the pollutant degradation and reduce its energy cost. For this reason, in the next step of this study, the application of voltammetric tools *in tandem* with chromatographic ones is performed to achieve this goal.

3.2. Application of DPV technique

3.2.1 Characterization of the HEF system

Preliminary experiments were carried out to obtain information on the direct reduction of iron from FeAS of HEF to get insight about the availability of Fe^{3+} into the reactor (Fig. 2).

As shown in Fig. 2a, at time 0, the characteristic peak for Fe(III) reduction at 0.092 V was observed (Bocos et al., 2017). In the first 15 min of HEF, this peak increased, being the peak current (i_p) 6 times higher than at time 0, and it shifted to more positive potential (c.a. 0.126 V). This increase continued up to 45 min, while the peak potential (E_p) remained almost constant around 0.140 V during this period of time. After 45 min, both i_p and E_p of the voltammetric peak of Fe(III) remained constant with values of about 2.01 µA and 0.137 V, respectively. Voltammetric kinetic data were obtained by monitoring this peak of Fe(III) released from the FeAS during the HEF and the rate constant was calculated by fitting the i_p, in µA, to the exponential first-order reaction. Fig. 2b illustrates the evolution of the

voltammetric peak of Fe(III) *versus* time plot, which follows a typically pseudo-first-order reaction and yields an observed rate-constant k_{obs} of (6.3±0.9) x10^{-2} min^{-1}, which is in relation to the rate-constant determined previously in section 3.1 (2.653 x10^{-2} min).

After initial characterization of the HEF system, and prior to monitor the treatment of the [IMes.HCl] by DPV, the voltammograms of Fe^{3+}, [IMes.HCl] and Cl^- were registered in order to identify the characteristic peaks of the reactants and the possible interactions between them, using Na_2SO_4 10 mM at pH 3 as electrolyte (HEF conditions) (Fig. 2c). The voltammogram of Fe^{3+} shows one peak centered at 0.038 V that is due to the reduction of Fe^{3+} to Fe^{2+}. The same behavior was observed for a mixture of Fe^{3+} and NaCl standard solution, where the complex $FeCl_4^-$ was formed, and the voltammogram also shows one peak with the same i_p but shifted to more positive potential (c.a. 0.209 V) compared with the peak of Fe^{3+} in Na_2SO_4 alone, being easier its reduction. In the same figure, the voltammogram obtained for the Fe(III) released from FeAS at 105 min of HEF is inserted just for comparison, and it shows that the E_p is shifted to more positive potential (c.a. 0.137) compared with the peak of Fe^{3+} alone. Besides, the insight of this Fig. 2c confirmed that the [IMes.HCl] was not electroactive at these working window potentials (Ni et al., 2017). In addition, the standard solution of [IMes.HCl] and Fe^{3+} shows a DPV curve with a broad peak at 0.119 V with lower i_p (52.6%) compared with the peak of Fe^{3+} alone. This fact can be attributed in part to the ionic interaction between the IL and Fe^{3+}, which makes its diffusion coefficient and its heterogeneous electron transfer rate constant smaller in the presence of IL (Patah et al., 2016).

The estimation of Fe(III) concentration released during the HEF treatment was done using the following equation for the linear fitting of calibration curve in the range of 0.05 mM to 1.3 mM (n =12): $i_p(\mu A)$ = (0.1±0.01) + (15.8±0.2) $C_{Fe(III)}$ (mM) (R^2 = 0.998), giving a LOD = 0.028 mM and a LOQ = 0.088 mM in Fe^{3+}. The estimated concentration of free Fe(III) in the reactor is around 0.120 mM (6.7 mg L^{-1}).

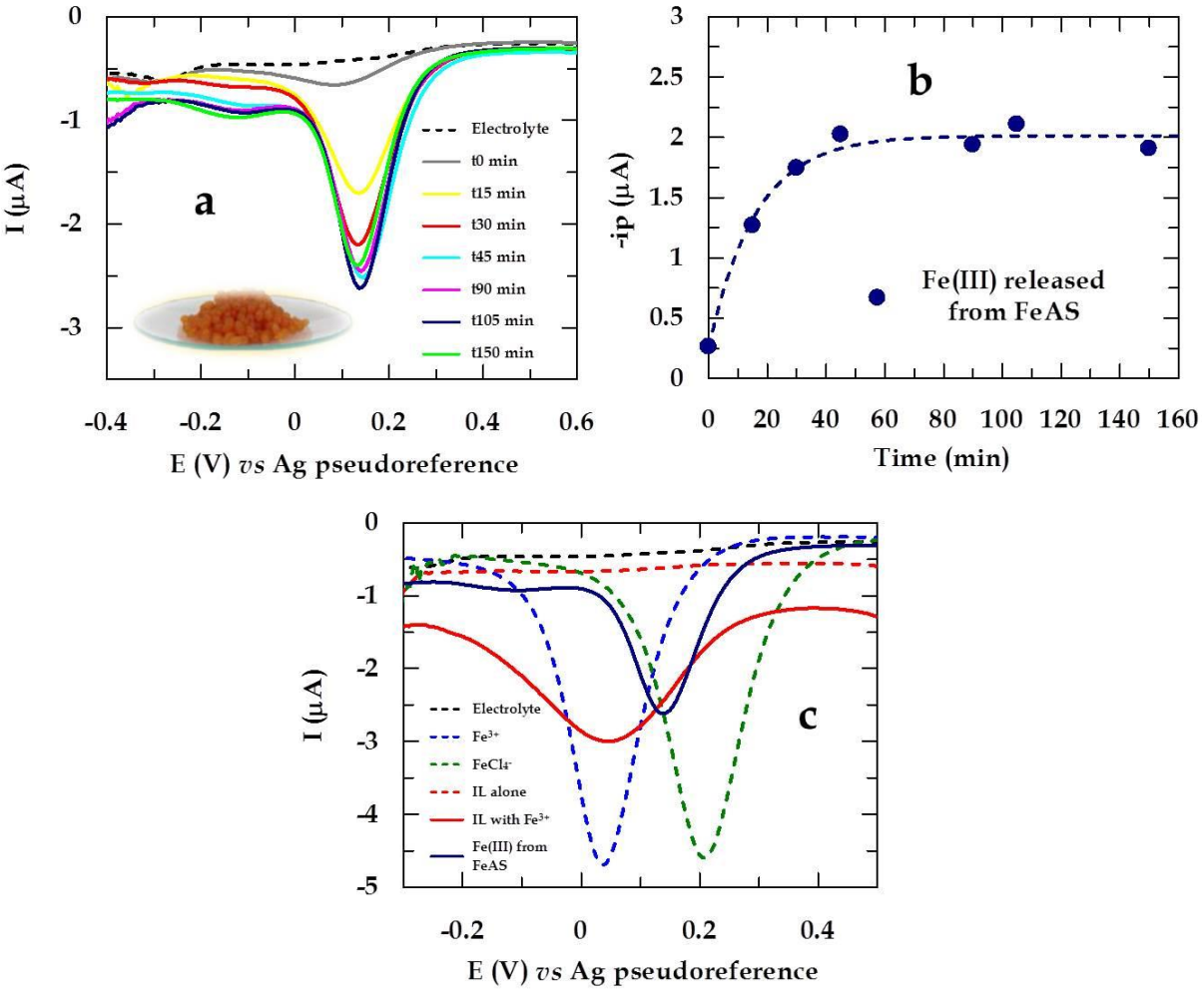

Fig. 2. DPV voltammogram recorded for samples took from HEF of Fe(III) immobilized in FeAS (5.013 g) in Na_2SO_4 10 mM at pH 3 as electrolyte (a); evolution of the i_p with time for the voltammetric peaks of Fe^{3+} reduction (b); residual current, $Fe_2(SO_4)_3xH_2O$ (0.25 mM), a mixture of $Fe_2(SO_4)_3xH_2O$ (0.25 mM) and NaCl (10 mM) to obtain the $FeCl_4^-$ complex, [IMes.HCl] (500 mg L^{-1}), a mixture of $Fe_2(SO_4)_3xH_2O$ (0.25 mM) and [IMes.HCl] (500 mg L^{-1}) and Fe(III) from FeAS during HEF at 105 min (c).

3.2.2 Evolution of HEF

As depicted in Fig. 3a, at the beginning of HEF treatment, one peak related to Fe^{3+} released from the FeAS was observed (see also Fig. 2a). In the next 90 min of treatment, this peak was

overlapped with a new broad peak centered at about -0.170 V, which i_p increased during the first 45 min, at the same time that was shifted to more positive potentials. This voltammetric behavior of the broad peak and the shoulder at higher potentials continued until 120 min, where the two peaks were perfectly distinguished. As it is shown in Fig. 2 and SM-3, there are two peaks: the first peak corresponds to the Fe^{3+} while the second one can be attributed to the complex formed by Fe and carboxylic acids generated as intermediates during the HEF, which E_p is dependent on the number of carbons in the carboxylic acid structure (Furia, 1972) and its complex formation constants (expressed as log β) (Reinders and de Minjer, 1938; Senthilnithy et al., 2008) (Fig. SM-3).

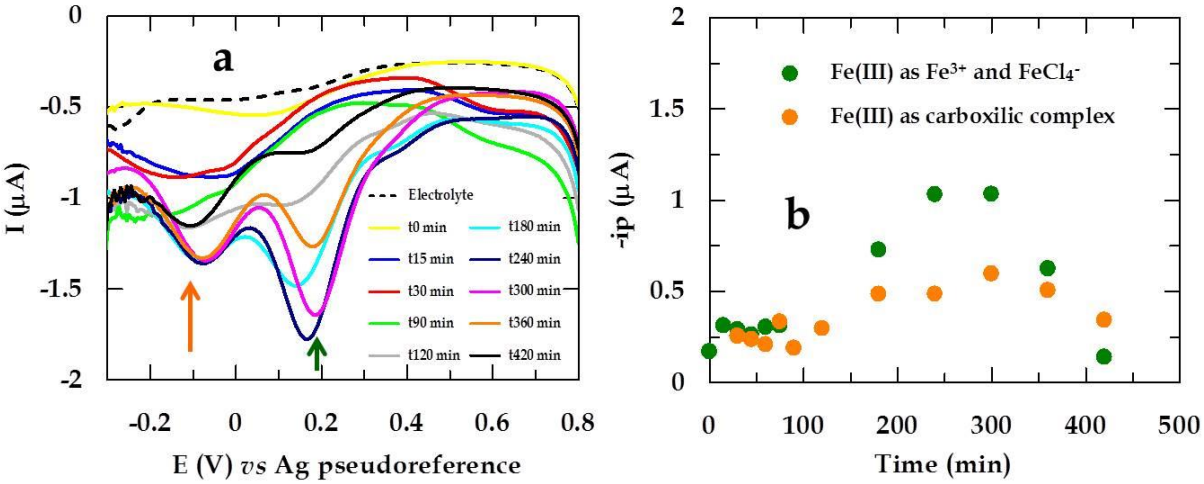

Fig. 3. DPV voltammogram recorded for samples taken from HEF treatment of [IMes.HCl] (500 mg L^{-1}) with Fe(III) immobilized in FeAS (5.022 g) in Na_2SO_4 10 mM at pH 3 as electrolyte (a) and the evolution of the i_p with time for the voltammetric peaks of Fe(III) (b) (see also Fig. SM-3).

At longer times of treatment (up to 120 min), the i_p of both peaks, Fe(III) and Fe-carboxylic complex (mainly for the formation of oxalic and oxamic acids intermediates, Fig. SM-3), increased continuously until reaching a maximum value at 300 min (Fig. 3b). After that time, the current of both peaks decayed progressively. In addition, both peaks were shifted to more

positive potentials. The peak potential shift of Fe(III) peak to about 0.2 V and the pale yellow color of the solution in the reactor can explain the formation of $FeCl_4^-$ complex.

In order to elucidate these findings by DPV, IC chromatography was applied (Fig. SM-4). As depicted in Fig. SM-4a, both inorganic (Cl^-, NO_3^- and SO_4^{2-} used as electrolyte) and organic anions (formic/glycolic/acetic that co-elute at about 4 min and oxamic/oxalic that co-elute at about 14.3 min) were eluted at different retention times. Representative IC chromatograms for the evolution of these ions during HEF at 5, 75 and 360 min of treatment are shown in Fig. SM-4b. As expected, the peaks of carboxylic acids start to be present from the beginning of the treatment. For chloride and nitrate, its concentration progressively increased up to 90 and 120 min, respectively, reaching again maximum values at 360 min, but sulphate was kept almost constant during the treatment, increasing slightly its concentration up to 300 min. This slight increase can be attributed to the sulphate ion leaching from FeAS.

These findings obtained from chromatography point out almost completely degradation of [IMes] cation and the release of free chloride and nitrate generated anions during the first 120 min, which is in good agreement with the results found during the degradation experiments by DPV (Fig. 3). In addition, these results indicate that carboxylic acids were released to the bulk of the solution and so their association with the free Fe^{3+} can be easier.

3.2.3 Evolution of carboxylic acids

Although IC results can help to understand the DPV voltammetric behavior, a more focused approach to know the concentration of each carboxylic acid was needed. For that, the detection and quantification of each carboxylic acid was performed by ion-exclusion HPLC. Fig. 4. shows the evolution of carboxylic acids released during HEF treatment. During the first 120 min, it can be seen that acetic, formic, malonic/maleic/glyoxylic, succinic, oxalic, oxamic and glycolic acids (in descending order of concentration found) were detected. After this time, only four carboxylic acids were detected and the evolution of its concentration was

as follows: acetic dropped down drastically, formic kept almost constant and the oxalic/oxamic couple decreased along the HEF treatment.

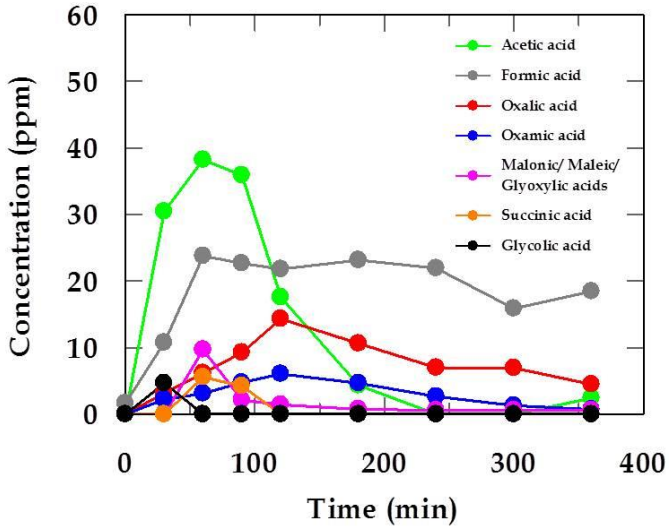

Fig. 4. Evolution of the released carboxylic acids during HEF treatment of [IMes.HCl] (163 mg L^{-1}) in 0.150 L in Na_2SO_4 10 mM at pH 3 obtained by HPLC.

The behavior for oxalic/oxamic acids may be due to the formation of a complex with Fe^{3+} (log β_1= 9.4 and 9.58, respectively) that are more stable than with formic (log β_1= 3.4). This fact explains the rise of i_p and the better defined shape of both peaks found by DPV up to 120 min given the formation of the Fe-carboxylic complex. This trend can be observed in Fig. 3b, where the formation of these complexes delays the degradation of carboxylic acids, which explains the decreasing of i_p in DPV, the increasing of nitrate concentration by IC (Fig. SM-4c) and the progressive decreasing of oxamic/oxalic acids concentration by HPLC (Fig. 4).

4. CONCLUSIONS

This study presents the results obtained by the application of the HEF process for the degradation of the [IMes.HCl] IL. A deep insight in the process with the study of operational parameters using the Box-Behnken experimental design allowed concluding the positive effect of current and FeAS dosage and their interrelation with the initial [IMes.HCl]

concentration used. Finally, the application of DPV technique elucidated the main degradation pathways of the [IMes.HCl]. This technique has demonstrated being a powerful tool for determining both Fe^{3+} release from FeAS and the moment when the [IMes.HCl] molecule was broken. At the same time, it provided relevant information about the evolution of the intermediates generated and its interactions with the Fe^{3+}, which were confirmed by chromatography.

Acknowledgments

This research has been financially supported by the Spanish Ministry of Economy and Competitiveness (MINECO) and European Regional Development Fund (Projects CTM2014-52471-R). The authors are grateful to MINECO, University of Vigo and Xunta de Galicia for the financial support of Dr Rosales, and PhD students Poza and Arellano, respectively. The authors are grateful to Pepe Lamas for his helpful hands in the laboratory.

References

Barhoumi, N., Labiadh, L., Oturan, M.A., Oturan, N., Gadri, A., Ammar, S., Brillas, E., 2015. Electrochemical mineralization of the antibiotic levofloxacin by electro-Fenton-pyrite process. Chemosphere 141, 250-257.

Barhoumi, N., Olvera-Vargas, H., Oturan, N., Huguenot, D., Gadri, A., Ammar, S., Brillas, E., Oturan, M.A., 2017. Kinetics of oxidative degradation/mineralization pathways of the antibiotic tetracycline by the novel heterogeneous electro-Fenton process with solid catalyst chalcopyrite. Appl. Catal. B: Environ. 209, 637-647.

Bocos, E., Pazos, M., Sanromán, M.A., 2016. Electro-Fenton treatment of imidazolium-based ionic liquids: kinetics and degradation pathways. RSC Adv. 6, 1958-1965.

Bocos, E., Pazos, M., Sanromán, M.A., 2014. Electro-Fenton decolourization of dyes in batch mode by the use of catalytic activity of iron loaded hydrogels. J. Chem. Technol. Biotechnol. 89, 1235-1242.

Bocos, E., González-Romero, E., Pazos, M., Sanromán, M.A., 2017. Application of electro-Fenton treatment for the elimination of 1-Butyl-3-methylimidazolium triflate from polluted water. Chem. Eng. J. 318, 19-28.

Dai, C., Zhang, J., Huang, C., Lei, Z., 2017. Ionic liquids in selective oxidation: catalysts and solvents. Chem. Rev. 117, 6929-6983.

Deive, F.J., Rodríguez, A., Varela, A., Rodrígues, C., Leitao, M.C., Houbraken, J.A., Pereiro, A.B., Longo, M.A., Sanromán, M.A., Samson, R.A., 2011. Impact of ionic liquids on extreme microbial biotypes from soil. Green Chem. 13, 687-696.

Egorova, K.S., Ananikov, V.P., 2014. Toxicity of ionic liquids: eco (cyto) activity as complicated, but unavoidable parameter for task-specific optimization. ChemSusChem 7, 336-360.

Furia, T.E., 1972. Sequestrants in foods. In: CRC Handbook of Food Additives. CRC Press, Boca Raton, FL, pp. 271-294.

Garcia-Segura, S., Lima, A.S., Cavalcanti, E.B., Brillas, E., 2016. Anodic oxidation, electro-Fenton and photoelectro-Fenton degradations of pyridinium- and imidazolium-based ionic liquids in waters using a BDD/air-diffusion cell. Electrochim. Acta 198, 268-279.

Gomez-Herrero, E., Tobajas, M., Polo, A., Rodriguez, J.J., Mohedano, A.F., 2018. Removal of imidazolium- and pyridinium-based ionic liquids by Fenton oxidation. Environ. Sci. Pollut. Res. (In press) https://doi.org/10.1007/s11356-017-0867-4

Guelfi, D.R.V., Gozzi, F., Sirés, I., Brillas, E., Machulek, A., Jr., de Oliveira, S.C., 2017. Degradation of the insecticide propoxur by electrochemical advanced oxidation processes using a boron-doped diamond/air-diffusion cell. Environ. Sci. Pollut. Res. 24, 6083-6095.

Iglesias, O., Fernández de Dios, M.A., Pazos, M., Sanromán, M.A., 2013. Using iron-loaded sepiolite obtained by adsorption as a catalyst in the electro-Fenton oxidation of Reactive Black 5. Environ. Sci. Pollut. Res. 20, 5983-5993.

Iglesias, O., Gómez, J., Pazos, M., Sanromán, M.A., 2014. Electro-Fenton oxidation of imidacloprid by Fe alginate gel beads. Appl. Catal. B: Environ. 144, 416-424.

Kalcikova, G., Zagorc-Koncan, J., Znidarsic-Plazl, P., Gotvajn, A.Z., 2012. Assessment of environmental impact of pyridinium-based ionic liquid. Fresenius Environ. Bull. 21, 2320-2325.

Lin, H., Oturan, N., Wu, J., Sharma, V.K., Zhang, H., Oturan, M.A., 2017. Removal of artificial sweetener aspartame from aqueous media by electrochemical advanced oxidation processes. Chemosphere 167, 220-227.

Meijide, J., Pazos, M., Sanromán, M.A., 2018. Heterogeneous electro-Fenton catalyst for 1-butylpyridinium chloride degradation. Environ. Sci. Pollut. Res. (In press) https://doi.org/10.1007/s11356-017-0403-6

Mena, I.F., Cotillas, S., Díaz, E., Sáez, C., Rodríguez, J.J., Cañizares, P., Mohedano, ÁF., Rodrigo, M.A., 2018. Electrolysis with diamond anodes: eventually, there are refractory species! Chemosphere 195, 771-776.

Morandeira, L., Álvarez, M.S., Markiewicz, M., Stolte, S., Rodriguez, A., Sanromán, M.A., Deive, F.J., 2017. Testing the true choline ionic liquids biocompatibility from a biotechnological standpoint. ACS Sustain. Chem. Eng. 5, 8302-8309.

Mousset, E., Oturan, N., van Hullebusch, E.D., Guibaud, G., Esposito, G., Oturan, M.A., 2014. Influence of solubilizing agents (cyclodextrin or surfactant) on phenanthrene degradation by electro-Fenton process – Study of soil washing recycling possibilities and environmental impact. Water Res. 48, 306-316.

Muñoz, M., Domínguez, C.M., de Pedro, Z.M., Quintanilla, A., Casas, J.A., Rodriguez, J.J., 2015. Ionic liquids breakdown by Fenton oxidation. Catal. Today 240, 16-21.

Muñoz, M., Domínguez, C.M., de Pedro, Z.M., Quintanilla, A., Casas, J.A., Rodriguez, J.J., 2016. Degradation of imidazolium-based ionic liquids by catalytic wet peroxide oxidation with carbon and magnetic iron catalysts. J. Chem. Technol. Biotechnol. 91, 2882-2887.

Ni, W., Liu, S., Fei, Y., He, Y., Ma, X., Lu, L., Deng, Y., 2017. The determination of 1-methylimidazole in room temperature ionic liquids based on imidazolium cation by cyclic voltammetry. J. Electroanal. Chem. 787, 139-144.

Ouiriemmi, I., Karrab, A., Oturan, N., Pazos, M., Rozales, E., Gadri, A., Sanromán, M.Á, Ammar, S., Oturan, M.A., 2017. Heterogeneous electro-Fenton using natural pyrite as solid catalyst for oxidative degradation of vanillic acid. J Electroanal Chem. 797, 69-77.

Patah, A., Bächle, J., Grampp, G., 2016. Cations/anions effects of imidazolium-based ionic liquids on the diffusion properties of iron- and ruthenium-bipyridine/phenanthroline complexes. Electrochim. Acta 219, 305-311.

Pęziak-Kowalska, D., Fourcade, F., Niemczak, M., Amrane, A., Chrzanowski, Ł, Lota, G., 2017. Removal of herbicidal ionic liquids by electrochemical advanced oxidation processes combined with biological treatment. Environ. Technol. 38, 1093-1099.

Reinders, W., de Minjer, C., 1938. The redox potentials of complex iron salts with the sodium salts of organic acids. Recueil des Travaux Chimiques des Pays-Bas 57, 594-603.

Richardson, S.D., Kimura, S.Y., 2017. Emerging environmental contaminants: challenges facing our next generation and potential engineering solutions. Environ. Technol. Innovation 8, 40-56.

Rossi, R.J., 2010. Applied biostatistics for the health sciences. John Wiley & Sons, New Jersey.

Senthilnithy, R., de Costa, M.D.P., Gunawardhana, H.D., 2008. The pKa values of ligands and stability constants of the complexes of Fe(III), Cu(II) and Ni(II) with some hydroxamic acids: a comparative study of three different potentiometric methods. J. Natl. Sci. Found. Sri Lanka 36, 191-198.

Simsek, E.B., Özdemir, E., Beker, U., 2013. Process optimization for arsenic adsorption onto natural zeolite incorporating metal oxides by response surface methodology. Water, Air, Soil Pollut. 224, 1614.

Sirés, I., Brillas, E., Oturan, M.A., Rodrigo, M.A., Panizza, M., 2014. Electrochemical advanced oxidation processes: today and tomorrow. A review. Environ. Sci. Pollut. Res. 21, 8336-8367.